General Features of Photoinduced Spin Dynamics in Ferromagnetic and Ferrimagnetic Compounds

T. Ogasawara,[1] K. Ohgushi,[2] Y. Tomioka,[1] K. S. Takahashi,[2] H. Okamoto,[1,3] M. Kawasaki,[1,4] and Y. Tokura[1,2,5]

[1]*Correlated Electron Research Center (CERC), National Institute of Advanced Industrial Science and Technology (AIST), Tsukuba 305-8562, Japan*

[2]*Department of Applied Physics, University of Tokyo, Tokyo 113-8656, Japan*

[3]*Department of Advanced Materials Science, University of Tokyo, Kashiwa 277-8561, Japan*

[4]*Institute for Materials Research, Tohoku University, Sendai 980-8577, Japan*

[5]*Spin Superstructure Project (SSS), ERATO, Japan Science and Technology Corporation (JST), Tsukuba 305-0046, Japan*

(Received 18 May 2004; published 3 March 2005)

Ultrafast photoinduced spin dynamics has been investigated by time-resolved magneto-optical Kerr spectroscopy for various ferromagnetic and ferrimagnetic compounds: $FeCr_2S_4$, $CoCr_2S_4$, $CuCr_2Se_4$, $CdCr_2Se_4$, $La_{0.6}Sr_{0.4}MnO_3$, and $SrRuO_3$. The temporal demagnetization process, which is observed commonly for all the compounds, essentially consists of two components: One is an instantaneous change which originates perhaps from multiple emissions of magnetic excitations during nonradiative decay of photoexcited carriers, and the other is a delayed response due to thermalization of the spin system. The time constant of the delayed change depends strongly on materials and is scaled with the magnetocrystalline anisotropy, indicating that spin-orbit coupling is a dominant interaction for this process.

DOI: 10.1103/PhysRevLett.94.087202 PACS numbers: 75.40.Gb, 78.20.Ls, 78.47.+p

The state-of-the-art time-resolved magneto-optical spectroscopy can provide a challenging arena to test the ultrafast manipulation of spin states in ferromagnets. In general, it is hardly anticipated that genuine photoexcitation can efficiently alter the spin state because of the selection rule of the optical transitions. Nevertheless, the pioneering study reported by Beaurepaire *et al.* [1] demonstrated that the subpicosecond demagnetization could be induced in a ferromagnetic Ni film by femtosecond photoexcitation. Since then, several studies have been performed on Ni and ferromagnetic alloys [2–7], as well as ferromagnetic transition-metal oxides [8,9], in all of which the photoinduced demagnetization dynamics have been successfully detected.

As for the mechanism of the photoinduced demagnetization, there have been proposed several scenarios. At first, in the study on the Ni film [1], the time evolution of the magneto-optical Kerr signal was analyzed using a phenomenological model including three interacting reservoirs (electron, spin, and lattice), and the importance of direct electron-spin interaction was suggested. In the subsequent studies on Ni [4] and the ferromagnetic alloy CoPt [7], the spin dynamics was deduced by the set of the time dependent magneto-optical Kerr Faraday signal, and consequently the ultrafast demagnetization was attributed to the close thermal contact of the spin system with the lattice system as well as with the electron system. In the studies of the ferromagnetic transition-metal oxides [8,9], the temperature dependence of the photoinduced demagnetization dynamics was elucidated in terms of the critical slowing-down effect. Thus, the microscopic mechanism of the photoinduced demagnetization has not been fully clarified yet. For an overall understanding, it is necessary to perform a more systematic study on a rich variety of materials by employing the same experimental approach.

In this Letter, we report the comprehensive study of time-resolved magneto-optical Kerr spectroscopy on spinel-type chromium chalcogenides, $FeCr_2S_4$, $CoCr_2S_4$, $CuCr_2Se_4$, and $CdCr_2Se_4$, as well as perovskite oxides $La_{0.6}Sr_{0.4}MnO_3$ and $SrRuO_3$. From the temperature and material dependence, it is revealed that photoinduced demagnetization is composed of two processes in common with all the materials studied here: a steplike instantaneous response and a delayed response. The steplike process is attributed to multiple emissions of magnetic excitations during nonradiative decay of photoexcited carriers, whereas the delayed process corresponds to thermalization of the spin system in contact with the electron-lattice system. The crucial importance of the spin-orbit interaction for the latter process is pointed out.

Chromium chalcogenide spinel MCr_2X_4 (M = Fe, Co, Cu, Cd, X = S, Se) varies its magnetic property with M ions. $FeCr_2S_4$ and $CoCr_2S_4$ undergo ferrimagnetic transitions at 170 and 230 K, respectively, in which the spins on the tetrahedral M sites and the octahedral Cr sites couple antiferromagnetically. In the case of $CuCr_2Se_4$ and $CdCr_2Se_4$, the Cr site spins show the ferromagnetic order below 430 and 130 K, respectively. The nominal valence of Cr in $CuCr_2Se_4$ is 3.5+, and consequently the compound shows metallic conduction. These materials are known to show a large magneto-optical effect [10–12]. Perovskite $La_{0.6}Sr_{0.4}MnO_3$, which undergoes a ferromagnetic transition at 360 K, is a typical ferromagnet associated with double-exchange interaction. Perovskite $SrRuO_3$, which exhibits good metallic conduction, undergoes a ferromagnetic transition at 150 K (in the form of an epitaxial thin

film). Magnetic structure, transport properties, Curie temperature T_C, and magnetocrystalline anisotropy constant K_1 (leading term for each crystal symmetry) at about the liquid He temperature [13–19] of the materials investigated here are summarized in Table I.

Photoinduced spin dynamics was investigated by femtosecond time-resolved magneto-optical Kerr spectroscopy. Changes in magneto-optical Kerr rotation θ and ellipticity η of the probe pulse were detected by a balance detection technique [8]. The pump and probe pulses were provided by an amplified mode-locked Ti:sapphire laser, combined with its second harmonic generation and parametric amplification. The pulse repetition rate was 1 kHz, and the typical temporal resolution of the system was ~200 fs. The photon energy of the probe pulse was selected so that the magneto-optical effect could optimally reflect the magnetization, usually at about the peak photon energy of the magneto-optical signal. An external magnetic field of ~0.25 T was applied normal to the surface by a permanent magnet. The chromium chalcogenide crystals were grown by a chemical transport reaction method, and their as-grown specular surfaces were used for optical measurements. A crystal of $La_{0.6}Sr_{0.4}MnO_3$ was grown by a floating zone method, and was polished and annealed for optical measurements. A thin film of $SrRuO_3$ with the thickness of 600 nm was fabricated by a pulsed laser deposition method on a $SrTiO_3$ substrate.

The time evolutions of the photoinduced changes in magneto-optical Kerr rotation $\Delta\theta/\theta_S$ and ellipticity $\Delta\eta/\eta_S$ are presented in Figs. 1(a)–1(f). Here, θ_S and η_S are the saturation values of θ and η, respectively, which were evaluated from the steady-state magneto-optical measurements. All the results exhibit strong temperature dependence, especially at about the Curie temperature T_C. By comparing these results with each other, one can see the general feature that the temporal behavior consists of five components as indicated in Fig. 1(g): (1) a *spikelike* component which rises instantaneously within the time resolution (~200 fs) after the photoexcitation and completes within a few picoseconds, (2) a *steplike* component which remains after completion of the spikelike component, (3) an *oscillation* component which has a period of several tens to hundreds picoseconds, (4) a *delayed* component which shows temporal growth in absolute magnitude after the photoexcitation observed prominently near T_C, and (5) a *decay* component with a time constant of about 10 ns.

As for the spikelike component (1), the similar temporal response is observed in the simultaneously measured photoinduced reflectivity change $\Delta R/R$ (not shown). Therefore, this component reflects the change not in magnetization but in reflectivity during the nonradiative decay of the photoexcited carriers. The oscillating component (3), which is usually observed at low temperatures, corresponds to the precession of the macroscopic magnetic moment induced by the change in anisotropic field upon photoexcitation [4,20,21]. The long-term (~10 ns) decay component (5) corresponds to the thermal diffusion process of bulk heating.

Figure 2(a) shows the temperature dependence of the height of the steplike component (2) for the respective materials. $La_{0.6}Sr_{0.4}MnO_3$ does not show a clear steplike response. The steplike component decreases towards the Curie temperature T_C, showing similar temperature dependence to that of the magnetization M presented in Fig. 2(b). This indicates that the photoexcitation randomizes a certain fraction of the spin system irrespective of initial spin

TABLE I. Magnetic structure, transport properties (M: metal, I: insulator), Curie temperature T_C, and magnetocrystalline anisotropy K_1. LSMO stands for $La_{0.6}Sr_{0.4}MnO_3$.

Material	Magnetism	M or I	T_C (K)	K_1 (J/m^3)
$FeCr_2S_4$	Ferri.	I	170	$(3–6) \times 10^5$
$CoCr_2S_4$	Ferri.	I	230	$(3–3.7) \times 10^4$
$CuCr_2Se_4$	Ferro.	M	430	$\sim -6.9 \times 10^4$
$CdCr_2Se_4$	Ferro.	I	130	$(0.4–4) \times 10^3$
LSMO	Ferro	M	360	$(0.1–1) \times 10^4$
$SrRuO_3$	Ferro.	M	150	$\sim 6.4 \times 10^5$

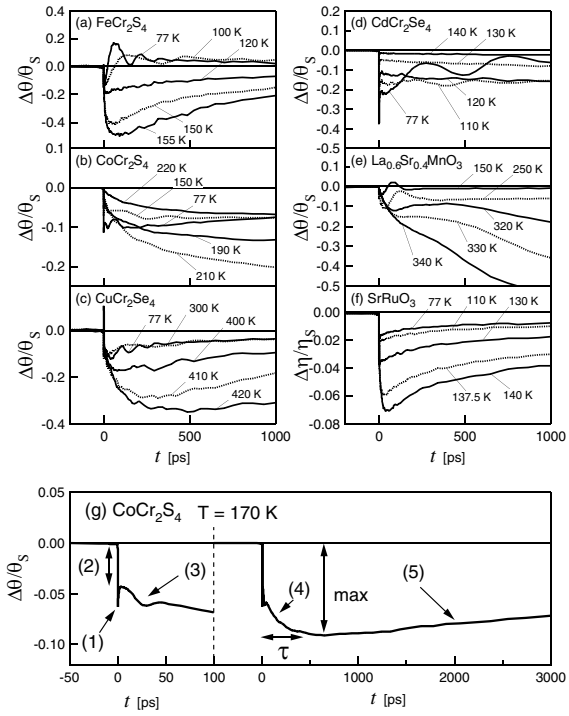

FIG. 1. Photoinduced changes in magneto-optical Kerr rotation or ellipticity. (a) $FeCr_2S_4$ (pump photon energy: 3.1 eV; probe photon energy: 1.9 eV; pump intensity: 85 μJ/cm^2), (b) $CoCr_2S_4$ (3.1 eV, 0.83 eV, 350 μJ/cm^2), (c) $CuCr_2Se_4$ (3.1 eV, 1.9 eV, 340 μJ/cm^2), (d) $CdCr_2Se_4$ (3.1 eV, 1.9 eV, 220 μJ/cm^2), (e) $La_{0.6}Sr_{0.4}MnO_3$ (1.5 eV, 3.1 eV, 500 μJ/cm^2), and (f) $SrRuO_3$ (1.55 eV, 3.1 eV, 30 μJ/cm^2). (g) Five characteristic components of time-resolved magneto-optical Kerr effect signal as exemplified for $CoCr_2S_4$: spikelike (1), steplike (2), oscillation (3), delayed (4), and decay (5) components, respectively.

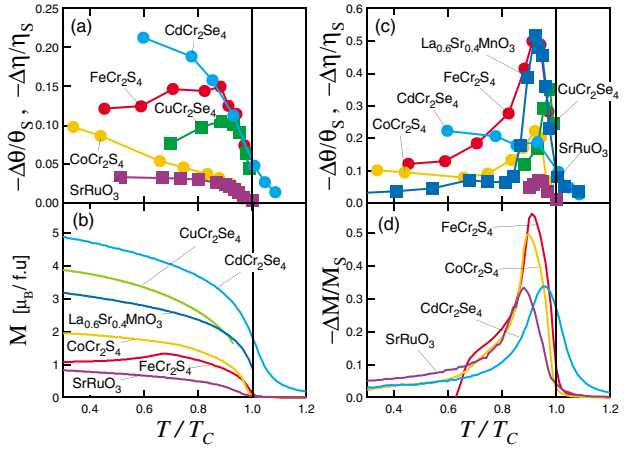

FIG. 2 (color). Normalized temperature (T/T_C) dependence of (a) the steplike component in the temporal response of the photoinduced demagnetization, apart from $La_{0.6}Sr_{0.4}MnO_3$ whose component is too small to discriminate from other components, (b) the magnetization M measured at 0.2 T, (c) the maximum of the photoinduced change in magneto-optical Kerr rotation (θ) or ellipticity (η) excluding the initial spikelike component and oscillation, and (d) thermally induced change of magnetization, $\Delta M/M_S = \frac{M(T+\Delta T)-M(T)}{M_S}$ with $\Delta T = 0.1T_C$, where M_S is the lowest-temperature saturation moment.

ordering. The fraction of the steplike demagnetization (10^{-2}–10^{-1} of the saturation magnetization) is 1 order of magnitude larger than the excitation densities (10^{-3}–10^{-2} per formula unit). This indicates that about ten sites of ferromagnetic spin ordering are destroyed by one absorbed photon. The onset of the steplike demagnetization is completed within the duration of the spikelike response which reflects the relaxation of the photoexcited carriers. This suggests that the steplike demagnetization process is associated not with the direct spin flip by the photoexcitation but with the successive emission of magnetic excitations such as magnons during nonradiative decay of photoexcited carriers.

The maximum value [see Fig. 1(g)] of $\Delta\theta/\theta_S$ or $\Delta\eta/\eta_S$, apart from the initial spikelike response and oscillating component, approximately corresponds to the magnitude of the delayed component (4). The temperature dependence of this value [Fig. 2(c)] shows a clear maximum at a temperature slightly below the Curie temperature, in contrast to the steplike component [Fig. 2(a)]. This behavior mimics the thermally induced change of the magnetization, $\Delta M/M_S = \frac{M(T+\Delta T)-M(T)}{M_S}$, which is shown in Fig. 2(d). Here, M_S is the lowest-temperature saturation moment. It clearly indicates that the delayed component corresponds to thermalization of the spin system.

Temperature dependence of the time constant τ for the growth of the delayed component [see Fig. 1(g)] is shown in Fig. 3(a). The τ shows a maximum slightly below the Curie temperature T_C. A similar phenomenon was reported and has been interpreted in terms of the critical slowing-down effect [8]. As the free-energy potential gets flattened near the Curie temperature, the time constant shows a critical increase about there. The possible reasons why τ does not show clear divergence in the present case are that an external field is applied to the sample and that the lattice temperature itself, which acts as a heat bath, varies with time.

The most prominent feature to be noticed is that τ varies more than 2 orders of magnitude depending on the materials. One can find a trend that a material with the stronger magnetocrystalline anisotropy (see Table I) shows the faster relaxation. To make this relation clear, the minimum and the maximum values of $1/\tau$ are plotted against magnetocrystalline anisotropy constant K_1 in Fig. 3(b). All the points are located between two dashed lines, showing a clear linear scaling relation between $1/\tau$ and K_1. This indicates the importance of the spin-orbit interaction in the thermalization process of the spin system. It is worth commenting on the pump-power dependence of the spin dynamics. The τ has been found to have pump-power dependence, which appeared as a horizontal shift of the curves in Fig. 3(a). This indicates that the change in the pump power leads to the change in the final spin temperature. Therefore it brings about no essential modification of the scaling relation presented here.

In addition, this scaling relation can be applied for both the metal and the insulator. The spin system is thermalized by contacting with the lattice vibration system and/or the electron system. Here, the *electron system* stands for the low-energy electronic excitations excluding spin excitations, i.e., quasiparticle excitations. The metal has the same lattice and electron systems as the heat bath, while

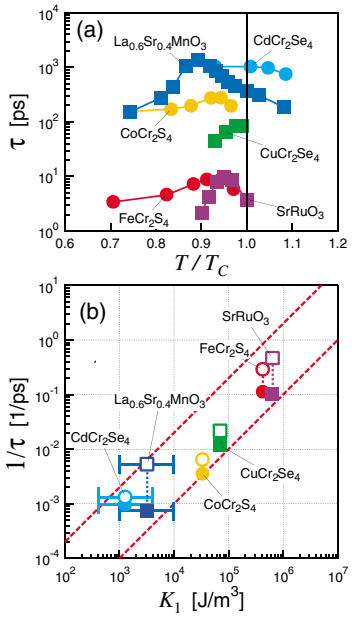

FIG. 3 (color). (a) Normalized temperature (T/T_C) dependence of time constant (τ) of the growing delayed component. (b) The inverse of the relaxation time constant ($1/\tau$) is plotted for the minimum and the maximum values against magnetocrystalline anisotropy constant (K_1). Dashed lines are the guides to the eyes.

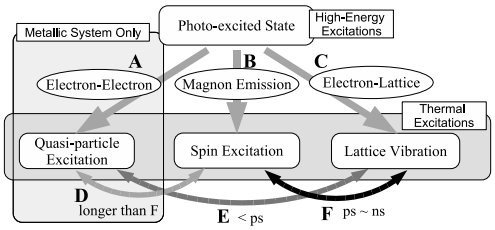

FIG. 4. Schematic diagram of the demagnetization process after photoexcitation.

the latter is absent in the insulator. The present result suggests that the spin-electron relaxation channel in the metal system does not make a major contribution to the thermalization of the spin system as compared with the spin-lattice channel. The obtained empirical relation [Fig. 3(b)] not only elucidates the microscopic origin of the delayed component, but also enables one to predict the dynamic nature of the materials from the features obtained by static measurements.

On the basis of the results presented above, the demagnetization process after photoexcitation can be interpreted in the scheme as presented in Fig. 4. High-energy photoexcited states are generated at first by a pump pulse, and then the excited states relax nonradiatively within a few picoseconds. During the nonradiative decay process, magnetic excitations (magnons) are emitted successively, and consequently a certain fraction of the magnetic order is randomized, giving rise to the steplike component (B in Fig. 4). The remaining energy of the photoexcited state is transferred to lattice dynamics (C), and also to quasiparticle excitation (A) in the metallic system. The thermal contact between the electron and the lattice systems (E) is relatively strong so that the electron and lattice systems reach the same effective temperature within a few picoseconds. At this moment, the effective temperatures of the spin and the lattice systems are, respectively, increased; however, these temperatures can be different because of the relatively small thermal contact between the spin and the lattice systems (F). Then the spin system relaxes to a new equilibrium by the thermal contact with the lattice system which is mediated by the spin-orbit coupling. The thermal contact between the electron and the spin systems (D) is not so close as that between the lattice and the spin system (F). Thus the charge degree of freedom does not give a significant contribution to the process of photoinduced spin dynamics.

As seen in Figs. 1(a)–1(f), the delayed component is not prominent at low temperatures. When the initial temperature is low, the increase of the effective temperature of the spin system immediately after the relaxation of photoexcited carriers, which is represented by the step component, appears to be higher than that of the lattice system. In this case, the magnetization monotonically recovers to the initial value. Near the Curie temperature, by contrast, the increment of the spin temperature (the step component) is diminished and becomes lower than the lattice temperature. Thus the magnetization continues to decrease after photoexcitation.

To summarize, we have investigated photoinduced spin dynamics in various ferromagnetic and ferrimagnetic compounds, $FeCr_2S_4$, $CoCr_2S_4$, $CuCr_2Se_4$, $CdCr_2Se_4$, $La_{0.6}Sr_{0.4}MnO_3$, and $SrRuO_3$, by the femtosecond time-resolved magneto-optical Kerr spectroscopy. As the general feature of the photoinduced spin dynamics, two types of demagnetization processes are observed: One is the steplike instantaneous demagnetization which is attributable to the multiple emission of magnetic excitations during nonradiative decay of photoexcited carriers. The other is the delayed, sometimes growing temporally in absolute magnitude, component which is attributed to thermalization of the spin system. The time constant of the delayed growing process is well scaled with the magnetocrystalline anisotropy, indicating that the thermalization of the spin system in the electron-lattice coupled heat bath is mainly mediated by spin-orbit interaction. These results give a guide to the material selection and design for the ultrafast spin control by photoirradiation.

[1] E. Beaurepaire, J.-C. Merle, A. Daunois, and J.-Y. Bigot, Phys. Rev. Lett. **76**, 4250 (1996).
[2] A. Scholl, L. Baumgarten, R. Jacquemin, and W. Eberhardt, Phys. Rev. Lett. **79**, 5146 (1997).
[3] J. Hohlfeld, E. Matthias, R. Knorren, and K. H. Bennemann, Phys. Rev. Lett. **78**, 4861 (1997).
[4] B. Koopmans, M. van Kampen, J. T. Kohlhepp, and W. J. M. de Jonge, Phys. Rev. Lett. **85**, 844 (2000).
[5] R. Wilks, N. D. Hughes, and R. J. Hicken, J. Appl. Phys. **91**, 8670 (2002).
[6] J. Hohlfeld, Th. Gerrits, M. Bilderbeek, Th. Rasing, H. Awano, and N. Ohta, Phys. Rev. B **65**, 012413 (2001).
[7] L. Guidoni, Eric Beaurepaire, and J.-Y. Bigot, Phys. Rev. Lett. **89**, 017401 (2002).
[8] T. Kise *et al.*, Phys. Rev. Lett. **85**, 1986 (2000).
[9] T. Ogasawara *et al.*, Phys. Rev. B **68**, 180407 (2003).
[10] R. Ahrenkiel, T. Coburn, and E. Carnall, Jr., IEEE Trans. Magn. **10**, 2 (1974).
[11] H. Bröndle, J. Schoenes, P. Wachter, and F. Hulliger, Appl. Phys. Lett. **56**, 2602 (1990).
[12] K. Sato, J. Phys. Soc. Jpn. **43**, 719 (1977).
[13] V. Tsurkan, J. Hemberger, M. Klemm, S. Klimm, A. Loidl, and R. Tidecks, J. Appl. Phys. **90**, 4639 (2001).
[14] A. Marais, M. Porte, I. Goldstein, and P. Gibart, J. Magn. Magn. Mater. **15–18**, 1287 (1980).
[15] I. Nakatani, H. Nose, and K. Masumoto, J. Phys. Chem. Solids **39**, 743 (1978).
[16] B. Hoekstra, R. P. van Stapele, and A. B. Voermans, Phys. Rev. B **6**, 2762 (1972).
[17] Y. Suzuki *et al.*, J. Appl. Phys. **83**, 7064 (1998).
[18] M. Ziese, H. C. Semmelack, and P. Busch, J. Magn. Magn. Mater. **246**, 327 (2002).
[19] A. Kanbayasi, J. Phys. Soc. Jpn. **41**, 1879 (1976).
[20] M. van Kampen *et al.*, Phys. Rev. Lett. **88**, 227201 (2002).
[21] Q. Zhang, A. V. Nurmikko, A. Anguelouch, G. Xiao, and A. Gupta, Phys. Rev. Lett. **89**, 177402 (2002).